View metadata, citation and similar papers at core.ac.uk
brought to you by CORE
provided by University of Bolton Institutional Repository (UBIR)

Novel ZnO nanorod films by chemical solution deposition for planar device applications

D.Singh[1], A.A.Narasimulu[1], L.Garcia-Gancedo[2], Y.Q.Fu[3], G.Shao[1] and J.K.Luo[1,4]*

[1]Inst. of Renewable Energy & Environ. Technol. (IREET), University of Bolton, Bolton, UK

[2]Electri. Eng. Div., Eng. Dept., University of Cambridge, 9 JJ Thomson Avenue, CB3 0FA, Cambridge, UK

[3]Thin Film Centre, University of the West of Scotland, Paisley, PA1 2BE, UK

[4] Dept. of Info. Sci. & Electron. Eng., Zhejiang University, Hangzhou 310027, P. R. China

Abstract: Smooth and continuous ZnO films consisting of densely packed ZnO nanorods (NRs) were synthesized using hydro-thermo-chemical solution deposition method which can be used for electronic device fabrication. These devices would have the novelty of high performance benefiting from the unique properties of the nanomaterials and can be fabricated on these films using conventional low cost planar process, as they have very smooth surfaces. Photoluminescence measurements showed that the nanorod films have much stronger band-to-band emissions than those from discrete ZnO NRs, hence have the potential for the development of ZnO light emission diodes and lasers etc. The nanorod films have been used to fabricate large area planar surface acoustic wave devices by conventional photolithography and demonstrated two well-defined resonant peaks and their potential for large area device applications. The chemical solution deposition method is a simple, reproducible, scalable and economic method. These nanorod films are suitable for large scale production and synthesis on cost-effective substrates promising for various fields such as sensing systems, renewable energy and optoelectronic applications.

Keywords: ZnO NRs, Smooth nanorod film, Planar structure, Photoluminescence, Surface acoustic wave

1. Introduction

Nanostructures such as nanodots, nanowires (NWs), nanorods (NRs) and nanotubes (NTs) have unique properties such as high mobility of carriers [1], high quantum confinement and efficiency for optoelectronics [2], excellent piezoelectric effect [3]. These structures have been intensively investigated and studied for the development of various electronic, optoelectronic, electrochemical and nanosystems [4- 9]. Most of the one-dimension-like nanostructures have randomly distributed crystal orientations, therefore, only those grown horizontally or vertically on the surface of the substrates are suitable for device fabrications. Horizontal NWs and NRs have been utilized to fabricate lateral structure devices such as field effect transistors [10], but special techniques are required to transfer or move them to specific locations for device fabrication. Vertically-aligned NWs and NRs are useful for the development of p/n junction-based devices such as laser diodes [11], light emitting diodes (LEDs) [12], nano-sensors and nano-actuators [13]. However, the development of nanomaterial-based electronic devices and nanosystems in a large scale is very limited. Firstly, it is extremely difficult to grow nanostructures on specified locations required for device fabrication, especially while using the conventional planar process. Secondly, most deposition methods, especially the solution-based ones, could not easily control the growth direction, crystal orientations, aspect ratio and densities of NWs and NRs, so that these fabricated devices generally have poor uniformity and reliability, and are unable to be used for many practical applications.

Figure 1(a) shows a schematic drawing of a typical method developed for fabricating devices with vertically-aligned discrete NWs or NRs [14,15]. As illustrated, it is difficult to control the number, orientation and dimensions of the NWs, hence the devices based on these NWs have large dispersion in properties, and poor uniformity and reliability, not suitable for practical applications. Although densely packed NWs such as carbon nanotubes (CNTs) have been realized [16], they are not continuous solid films but have voids and gaps between CNTs, therefore they are not suitable for device fabrication using planar process. Furthermore, it requires additional process to fill the gaps of the nanomaterials and planarization processes such as chemical-mechanical polishing or etching back to make a smooth surface for fabricating the top contact electrodes, followed by removal of the filling if necessary. The whole process is very complicated.. Therefore, it is of great importance to develop a new technique for fabricating densely packed, continuous nanomaterials. The concept of using such a new type of NRs for device fabrication is schematically illustrated in figure 1(b) for vertical structure devices and in figure 1(c) for planar structure devices. Planar structure devices such as field effect transistors (FETs) can be directly fabricated on these nanomaterial films, while vertical structure devices such as LEDs and lasers can be fabricated using planar process, and finally the materials outside the device areas can be removed

if necessary. The novelties of these devices are that they will inherited the peculiar and unique properties of the nanomaterials used, and can be fabricated using conventional, low cost planar process such as photolithography instead of e-beam writing technique etc. We have recently successfully developed a continuous film packed with dense nanorods [17], and demonstrated that this type of smooth films can be useful for device fabrication in large scale by conventional photolithography.

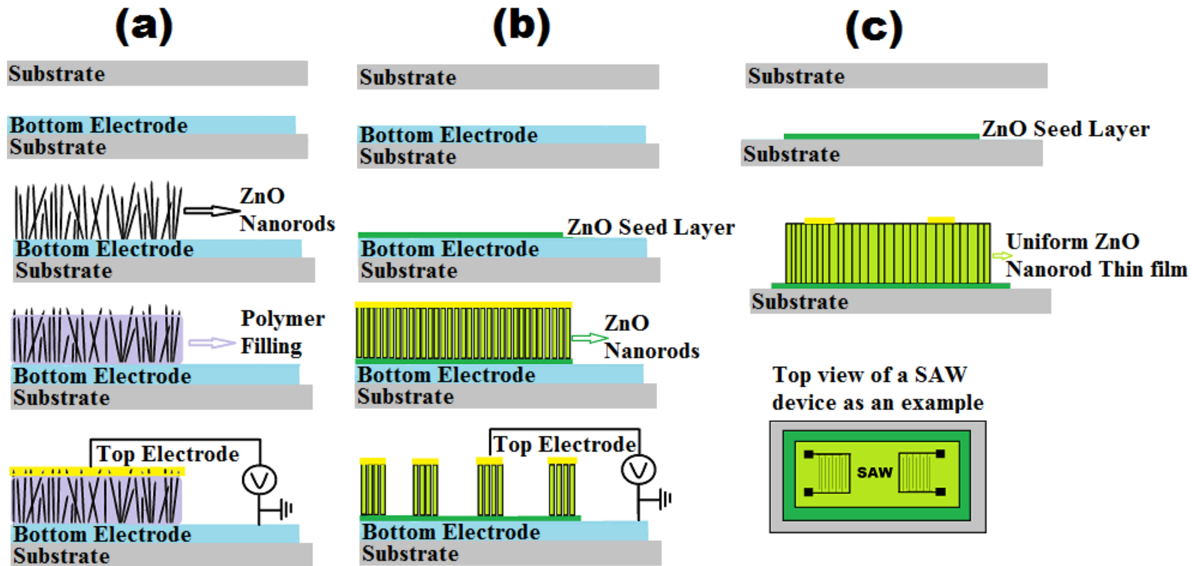

Figure 1. Schematic view of electronic devices made from discrete and continuous nanomaterial films. (a) a typical process used to fabricate devices with discrete nanomaterials and a concept for new nanorod films-based vertical (b) and lateral (c) structure devices that can be fabricated by traditional photolithography process.

ZnO is a unique material with properties suitable for fabrication of electronic and optoelectronic piezoelectric devices such as lasers and LEDs [18-21], surface acoustic wave (SAW) devices and bulk acoustic wave (BAW) resonators [22-28], piezoelectric transducers for microfluidics and lab-on-a-chip [29,30], transparent electronics [31], as well as various sensors for sensing various parameters such as temperature, pressure, force, torque and bio substances [32,33]. ZnO NRs have recently attracted great attentions for development of nano-generators through piezoelectric effect [3,34]. However, this requires a special contact electrode scheme hanging over the discrete NRs with no direct contact, and also a complicated process which will limit its fabrication and application. Further to our previous work in Ref [17], here we report a systematic investigation on the synthesis and characterization of smooth and continuous ZnO films which consist of tightly packed ZnO NRs.

Various ZnO nanostructures can be grown by many methods such as metal–organic chemical vapor deposition [35], molecular beam epitaxy [36], pulsed laser deposition [37], sputtering [38,39], atomic layer deposition (ALD) [40], and chemical solution deposition (CSD) [41] etc. The CSD method has

many significant advantages over the other deposition techniques owing to its nature of low cost and low temperature processing [42]. Various ZnO nanostructures such as nanoflowers, nanoneedles, nanocastles and NRs have been synthesized using different solutions including zinc nitrate ($Zn(NO_3)_2$) and hexamethylenetetramine (HMTA, $C_6H_{12}N_4$) [39] or NH_4OH [43] as precursors under different conditions. At a suitable growth condition, discrete hexagonal NRs with diameters from a few nanometers (nm) to a few hundreds of nm can be grown [44- 45]. We will show the morphology of the CSD-grown ZnO nanostructures can be changed significantly from discrete NRs to a continuous film with a smooth surface under an optimal condition. These thin films can be used for the fabrication of large area planar structures such as SAW devices with good performance.

2. Experimental details

All the solutions were prepared using deionized (DI) water (~18 MΩ·cm). All chemicals used for the synthesis solutions were purchased from Sigma Aldrich Co. Ltd with analytical reagent grade without further purification for experiments.

2.1 Aqueous solution growth

The precursor solutions were prepared by mixing zinc nitrate ($Zn(NO_3)_2 \cdot 6H_2O$ with 99.9% purity) and HMTA (99.9% purity) with DI water. The volume ratio of the two chemicals was fixed at 1:1, and their concentrations in solutions were varied from 0.03 to 0.12 M to investigate the effect of chemical concentrations on the morphology of the ZnO materials.

ZnO NRs were grown on ZnO seeded substrate. The seed layer of ZnO was deposited on (100)-oriented silicon (Si) substrates with a thickness between 20 and 70 nm. The seed layers were deposited by either RF magnetron sputtering or atomic layer deposition (ALD) methods. Before the deposition, the Si substrates were ultrasonically cleaned in acetone and ethanol for 10 min, followed by rinsing in DI water. They were dried with nitrogen gas before being introduced into the deposition system for ZnO layer deposition. For the sputtering deposition, the seed ZnO thin films were deposited at room temperature using a Zn target (99.999% purity) in a gas mixture of Ar and O_2. For the ALD deposition, diethyl zinc (DEZ) was used as the precursor as the zinc source and DI water was used as the oxidation source. The growth cycle involved precursor exposures and N_2 purges following the sequence of DEZ/N_2/H_2O/N_2 [50]. The ALD growth temperature for the seed ZnO layer deposition was 200 °C.

The CSD was carried out at temperatures from 40 °C to 95 °C in a glass beaker placed in water bath by immersing the pretreated substrates with the top side down in the precursor solutions with a volume of 50

ml. The growth time was 4 hrs for most samples. Finally, the grown samples were thoroughly washed with DI water to remove any residual salt and dried under a stream of N_2 gas.

2.2 Characterization

Surface morphology of the NRs and films were studied using a scanning electron microscopy (SEM, Hitachi S-3400) and the surface roughness were characterised using an atomic force microscopy (AFM, Agilent 5500SPM). The purity and composition of the samples were analysed using Kratos Axis Nova XPS system with an Al Kα (1486.6 eV) source. Crystalline structure of the nanorod films was determined by X-ray diffraction (XRD) analysis using a Rigaku diffractometer. The photoluminescence (PL) spectra of the samples at room temperature were determined with Perkin-Elmer LS-55 spectrophotometer equipped with a Xenon flash lamp. All the measurements were carried out under the excitation of 300 nm. Furthermore annealing of the ZnO NRs was carried out at temperatures from 200 °C to 500 °C for one hour in air to investigate its effect on the PL properties of the ZnO nanomaterials.

2.3 SAW device fabrication and characterization

SAW devices on NRs films were fabricated by standard deep UV photolithography process. The ZnO nanorod films with a thickness of ~4 µm were used for SAW device fabrication. SAW devices consist of 30 pairs of interdigitated transducer (IDT) fingers. The aperture of IDTs is 4900 µm, the spatial periodicity (wavelength) is 64 µm and the distance between the two IDT electrodes is 4 mm. Aluminum (Al) of ~100 nm thickness was used for IDT electrodes which were formed by thermal evaporation and lift-off process. The transmission characteristics of the SAW devices were measured using an Agilent E5061A Network Analyzer.

3. Results and discussions

3.1 Concentration effect

Figure 2 shows the SEM images, showing the morphological transformation of ZnO nanostructures from discrete NRs to a continuous and dense nanorod film when the chemical concentrations of zinc nitrate and HMTA (the ratio of zinc nitrate to HMTA is one, same for all concentrations stated hereafter) were varied, with a fixed growth temperature of 90 °C and growth duration of 4 hrs. The ZnO seed layer was deposited by sputtering with a thickness of 65 nm. The aspect ratio (defined as the width to the length) of the NRs increases gradually and the morphology changes from discrete one-dimensional nanorod structures to a dense two-dimensional film when the precursor concentrations were changed from 0.03 M

to 0.12 M. Figure 2(e) shows the top surface of the dense ZnO nanorod film. The surface crystals are well coalesced together to form a smooth surface, free of voids and gaps. The top of the ZnO NRs is featured by hexagonal structure.

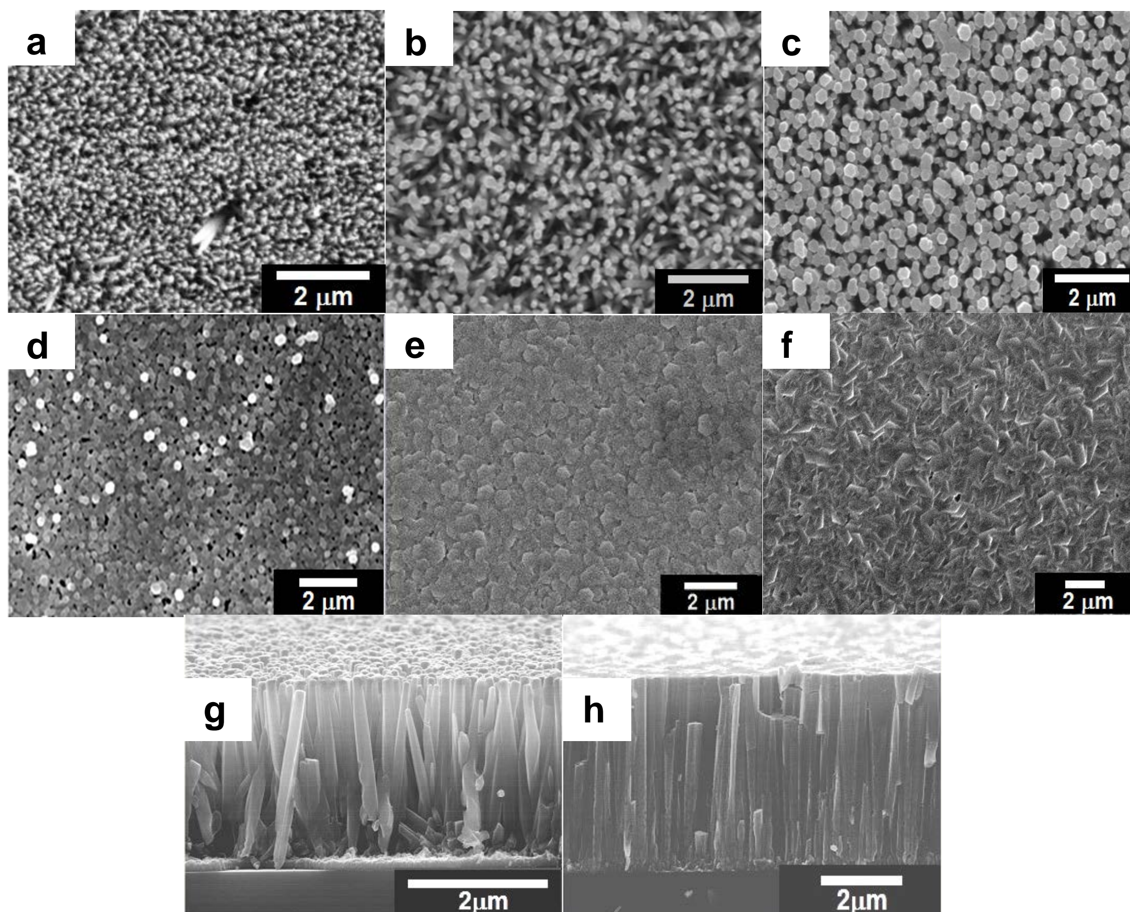

Figure 2. SEM images of the surface and cross-sectional view of the synthesized NRs at different molar concentrations of zinc nitrate and HMTA (the ratio of zinc nitrate to HMTA is one), (a) 0.03 M, (b) 0.05 M, (c) 0.06 M, (d): 0.07 M, (e) 0.10 M, (f) 0.12 M. The growth temperature and time were 90°C and 4 hrs. (g) and (h) show the cross sections for the films grown at 0.06 M and 0.1 M . All films were grown on 65 nm sputtered seed layer.

Chemical concentration has a significant effect on the morphology of the nanorod film [51]. The change of morphology and structure of ZnO films is attributed to the change in solubility of the salts which promotes the dissociation of HMTA, resulting in the increase of the $[OH^{-}]$ (or pH value) concentration in the solution. This accelerates the growth of ZnO NRs, increasing their size and improving the vertical orientation [52]. At low molar concentrations of ≤ 0.06M, the films either consist of discrete NRs or show many voids in the film as observed by many researchers, which are caused by the disoriented NRs as shown in figures 2(a) and 2(b). With increasing molar concentrations at ≥ 0.07M, the density of the NRs

increases and the steric hindrance [53,54] takes effect where the adjacent NRs tend to obstruct the normal growth thus contributing towards well oriented thin film structure with a uniform and smooth surface as shown in figures 2(c), 2(d) and 2(e). However, it was found that by further increasing the precursor concentrations, the aspect ratio of the NRs changes so significantly that uneven flake-like structures are formed, contributing to a rougher surface with voids as shown in figure 2(f). Figures 2(g) and 2(h) present a cross sectional view of the films as shown in figures 2(c) and 2(e).

Figure 3 shows the root mean square (RMS) roughness of the nanorod films as a function of precursor concentrations at a constant growth time of 4 hrs at 90 °C, measured by AFM. At a concentration of 0.1 M for both the zinc nitrate and HMTA precursors, a uniform surface with the lowest RMS roughness value of 4.5 nm was obtained over an area of 4 x 4 μm, showing an optimal precursor concentration for the synthesis of such uniform nanorod thin films.

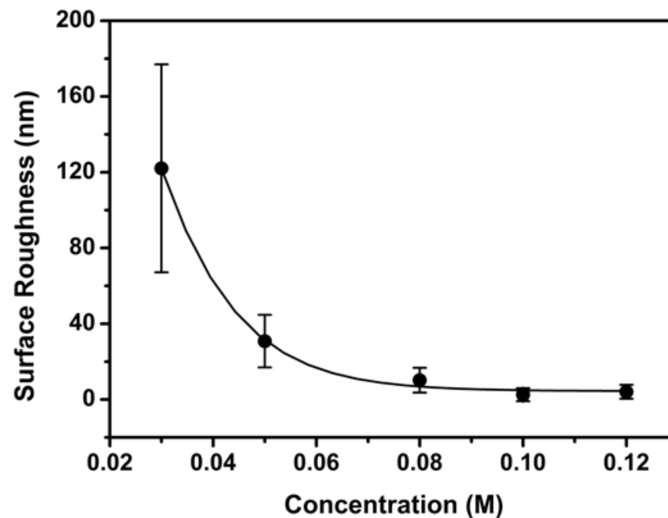

Figure 3. RMS roughness of the nanorod films at different precursor concentration measured by AFM. For samples with concentrationa less than 0.03 M, NRs are discrete and totally separated from each other, while others are films either smooth or having voids and gaps. The ones with the concentration of 0.1 M have the smoothest surface less than 5 nm. Sputtered seed layer for all the samples measured.

3.2 Effect of temperature

Temperature has a significant effect on the morphology and structure of the NRs. No ZnO nanostructures were grown on the seed layer at a growth temperature below 40 °C, and irregular nanostructures were formed for the samples grown at a temperature between 50 and 70 °C. As shown in figure 4, at a temperature of 75 ^{o}C, the NRs are discrete and separated from each other. The nanorod growth rate increased with the temperature, and eventually a smooth and dense nanorod film was obtained at about 90

°C. Further increase of temperature to 95 °C generally resulted in a minor increase in the surface roughness, possibly due to the increased anisotropic growth of the NRs [43].

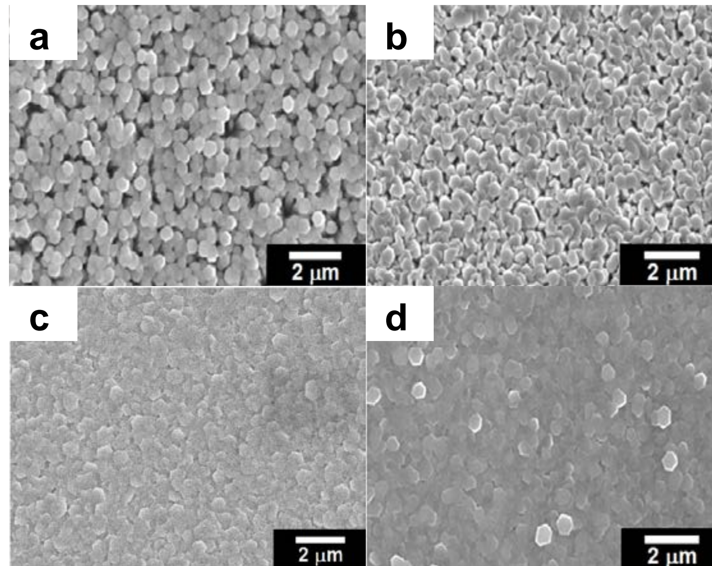

Figure 4. Evolution of ZnO nanorod films on temperature change. The precursor concentrations are 0.1M, and the temperature is (a) 75, (b) 80, (c) 90 and (d) 95 °C respectively. All samples were grown on 65 nm sputtered seed layer**.**

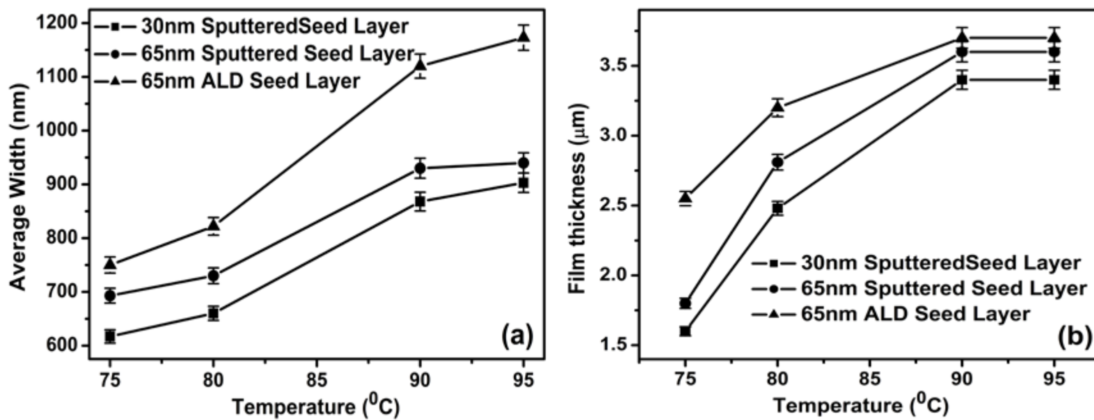

Figure 5. Temperature dependence of (a) axial and (b) lateral growth of ZnO NRs on seed layers deposited by sputtering and ALD depositions with different thickness. The precursor concentrations were 0.1 M for all the experiments.

Figure 5 shows the dependence of nanorod diameter (the largest diameter of a hexagon) and length (equivalent to the film thickness) on growth temperature for different seed layer thickness. The precursor concentrations for all these experiments were set to be 0.1 M. The average length of the NRs increases

significantly with the temperature up to 90 °C, but remains unchanged as the temperature was further increased to 95 °C. This implies that the growth rate along (0002) direction is more sensitive to temperature compared to those along (10-10), (10-11) or (10-12) directions as will be discussed later.

3.3 Effect of seed layer

The ZnO seed layer has a pronounced effect on the morphology and growth rate of the nanorod films [55]. Large numbers of ZnO nanoparticles serve as crystal seeds which promote faster growth, while a seed layer with highly textured ZnO nanoparticles could provide a good platform for growth of NRs with *c*-axis preferred orientation as the hexagonal rods are polar and have relatively large surface energy. Figure 6 shows the surface morphology of films grown on the ZnO seed layers deposited by sputtering or ALD with different thicknesses at the optimal growth condition (0.1 M concentrations and 90 °C, same hereafter). From the top and cross-sectional views of the SEM images, the obtained ZnO nanorod arrays have an improved structural orientation with the increase of seed layer thickness. With a thin seed layer, the size and number of the nucleus are limited and the crystal orientations would be random which is typically observed in physical vapour depositions [56]. These lead to a slow growth of the NRs with smaller diameters and more random crystal orientations as shown in figure 6(b). A thicker seed layer could provide a larger size of the nucleus with well formed crystal orientations, the growth rate of the NRs increases, contributing to the larger aspect ratio of the nanorod as shown in figure 6(d). This can be explained as follows: the initial layer of a sputtered seed layer has fine crystal structures with randomly distributed crystal orientation and the crystals become larger with a preferential orientation of (0002) as the sputtered layer becomes thicker [56].

On the other hand, the ALD grown layers have a smoother surface, smaller roughness and more uniform thickness, but the crystal is dominated by fine structure grains with some amorphous phases [57]. These could increase the number of nucleus, leading to the growth of denser nanorod films. The variation of the diameter and length of the NRs with the different seed layers is summarized in figure 5. The thicker the seed layer, the larger and longer NRs are for the same temperature and concentrations used.

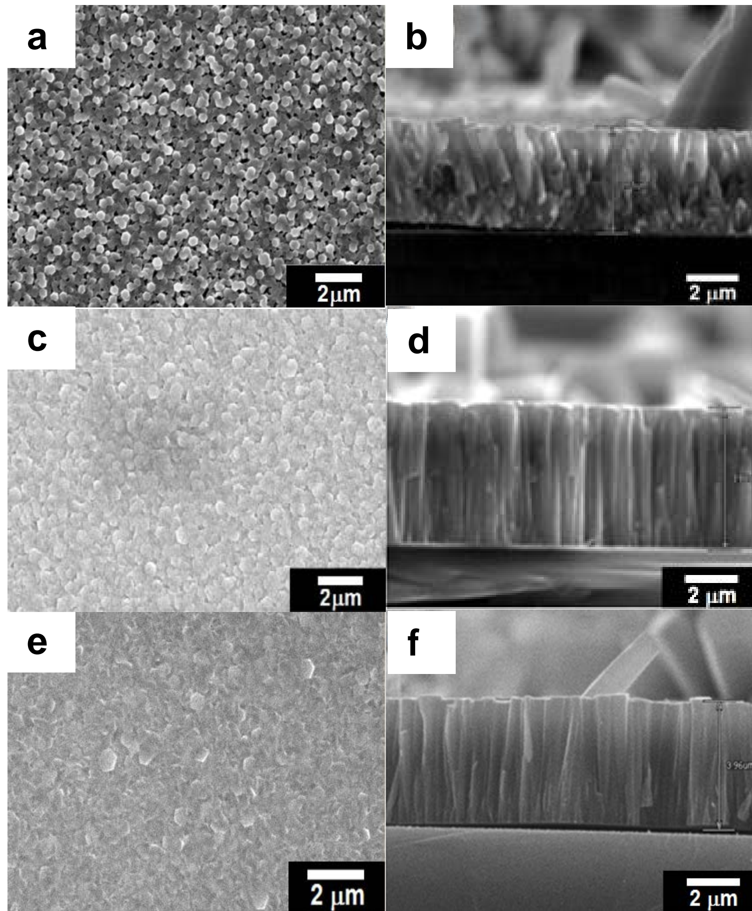

Figure 6. SEM images of ZnO nanorod films showing both the surface and cross-section. The films were grown at optimal condition of a zinc nitrate:HMTA molar ratio of 0.1 M : 0.1 M, 90 °C on seed layers of (a) (b) 30 nm and (c) (d) 65 nm deposited by sputtering, and (e) (f) 65 nm deposited by ALD.

The RMS roughness of the seed layers and the nanorod films were characterized using AFM with examples shown in figure 7. The RMS roughness of the 65 nm seed layers deposited by sputtering and ALD are 2.13 nm and 1.81 nm, respectively. The corresponding roughness of 4 μm thick nanorod films grown on the sputtering and ALD seed layers are 4.26 nm and 2.55 nm, respectively. It is worth to mention that the roughness of the nanorod films are smaller than most of ZnO films deposited by physical vapour deposition methods such as sputtering (where the surface RMS roughness values typically varied from 1.5 nm for 250 nm thick films to 20-100 nm for 4-5 μm thick film) [58] and laser ablation etc. The results indicate that the obtained nanorod films have good uniformity and smooth surface which ensure the fabrication of electronic devices by the planar process without the need for polishing process.

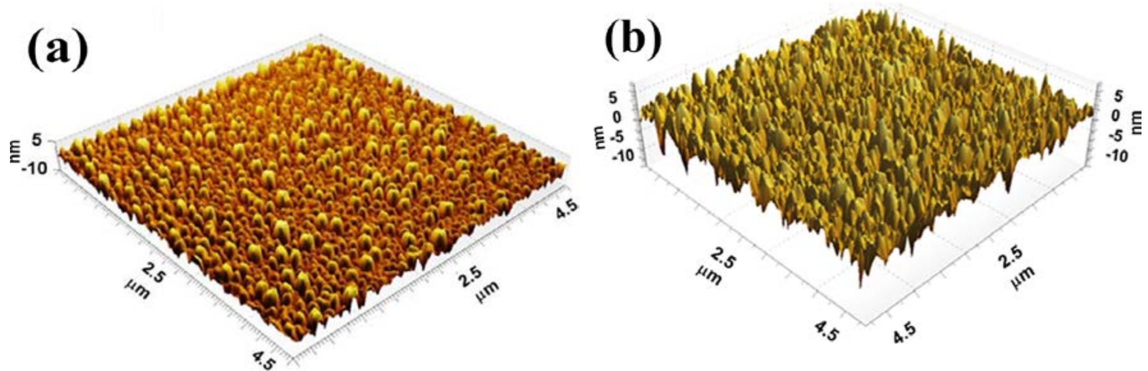

Figure 7. Surface images of the ZnO (a) ALD seed layer and (b) a 4 µm nanorod film growth on an ALD seed layer measured by AFM showing very small roughness RMS of 1.81nm and 2.55nm, respectively.

3.4 Time dependence of the growth

The film thickness (the length of the NRs) is roughly linearly related to the growth time as shown in figure 8. The average growth rate is ~800 nm·hr^{-1} for the optimal growth condition. Afterwards, the chemical concentrations tend to be exhausted, leading to a decreased growth rate. Eventually, growth stopped after 5-6 hrs due to the depletion of the chemical solutions. The growth resumes once it was replaced with a fresh growth solution. Smooth and dense films can grow without apparent voids and particles, and the length of the NRs has an excellent uniformity in the range of 95% across the samples of the size about 5 x 5 cm checked by SEM, except near to the edges.

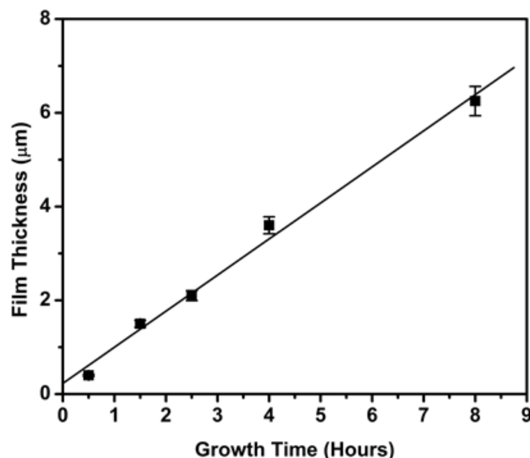

Figure 8. Dependence of ZnO nanorod length on the growth time at a constant temperature of 90 °C and precursor concentrations of 0.1 M, showing a linear relationship.

3.5 Material properties

To study their purity and composition, ZnO NRs and thin films synthesized using the solution growth method were characterized by XPS. Figure 9(a) shows full XPS spectrum of nanorod and thinfilm. The only identified elements are Zinc, oxygen and carbon (from surface contamination and adsorption), no traces of other elements were detected, indicating good purity of the material synthesized. Figure 9(b) shows well resolved peaks at 1022 and 1045 eV corresponding to the doublet of Zn $2p^{3/2}$ and Zn $2p^{1/2}$ respectively, which can be attributed to the formation of hexagonal ZnO NRs. The asymmetric O-1s peak in Fig. 9(c) was deconvoluted by two sub spectral components corresponding to Zn-O (530.8 eV) and Zn-OH species (532.2 eV), The peak at at 530.8 eV can be indexed to O^{2-} in the ZnO, whereas the weaker shoulder peak at about 532.2 eV is due to chemisorbed oxygen caused by the hydroxyl groups, which corresponds to the O–H bonds.[59] The XPS valance band spectrum consists of a large and sharp peak at ~11eV and is believed to have originated mainly from the d states of Zn sites. The upper valance band structures at 2-8eV are attributed to the p states at O sites while the small structure at ~22eV comes from the O 2s states.

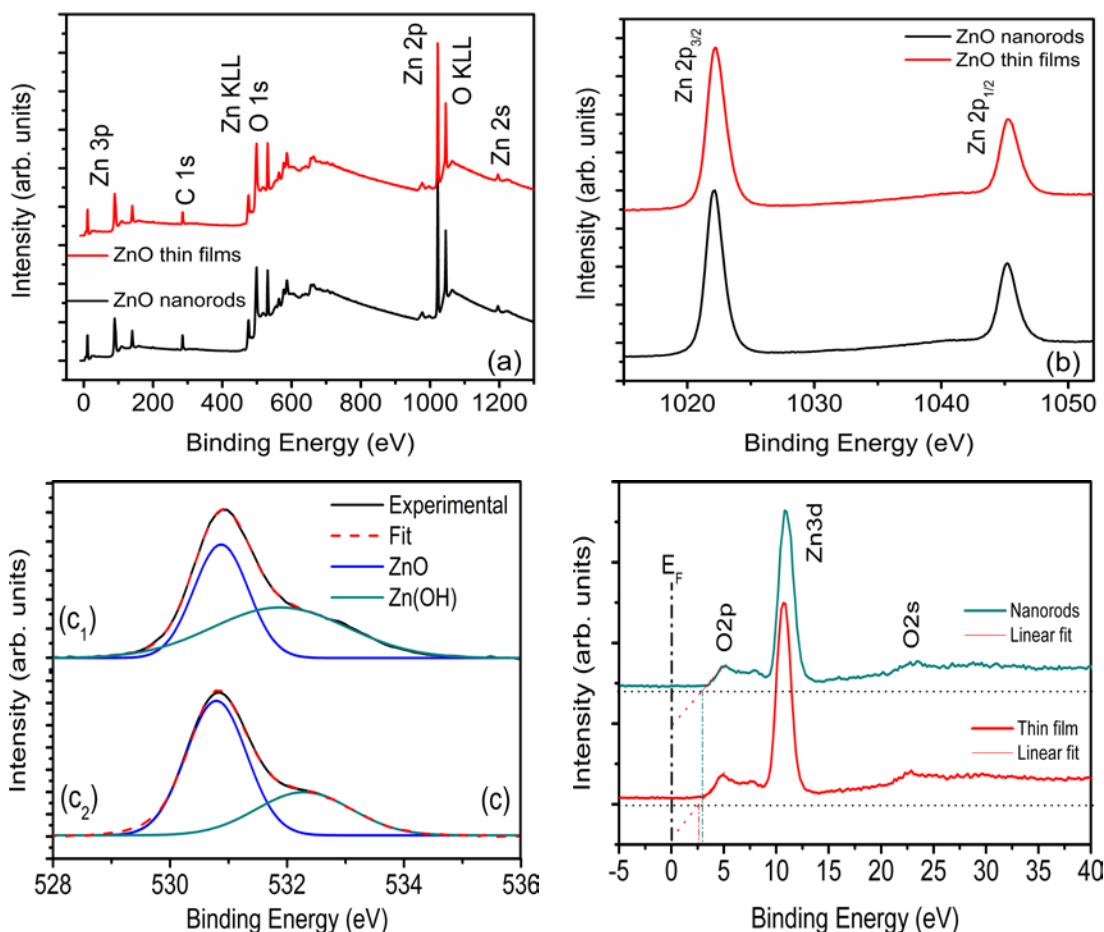

Figure 9. (a) Wide energy survey scan of ZnO NRs and thin films (b) Zn 2p spectrum (c) O1s core level spectrum of ZnO NRs (C_1) and ZnO thinfilms(C_2). (d) Valence band spectra of ZnO nanorods and thinfilms.

Figure 10 is the XRD curves for the films grown at different conditions. XRD analysis showed that both the discrete NRs and the nanorod films are the wurtzite structure of ZnO. The strong diffraction peak at 34.2° corresponds to the (0002) ZnO plane. This is because the *c*-plane perpendicular to a substrate is the most densely packed and thermodynamically favorable plane. The peak intensity of the dense film (65 nm ALD seed layer, precursor concentrations of 0.1 M) is much larger than that of the discrete NRs (30 nm ALD seed layer, precursor concentrations of 0.1 M). Growth along the other orientation of (10-10), (10-11) or (10-12) directions has not been observed. The intensity for the peak of (10-13) crystal orientation is relatively larger for the discrete NRs, and becomes smaller for the nanorod films, manifesting the preferential (0002) orientation for the films with a suppressed growth in other directions. The full-width at half maximum values decreases from 0.22 to 0.16 with increase in precursor concentration. This indicates that the film grains after their coalescence grow mainly in the direction normal to the substrate surface.

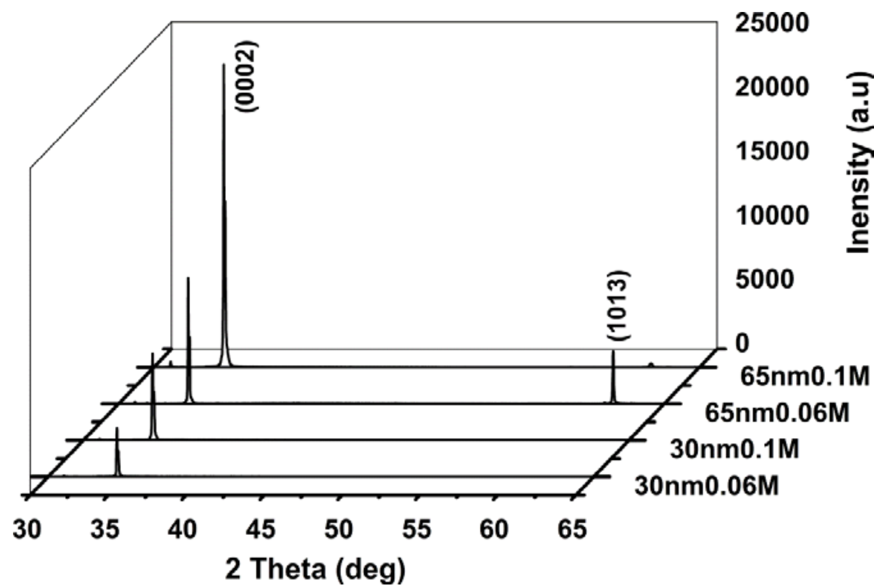

Figure 10. XRD results of ZnO nanorod materials grown at two different ALD seed layer thicknesses of 30nm and 65nm and at different precursor concentrations of 0.06M (NRs) and 0.1M (thinfilm) as shown in figure 2.

ZnO NRs have been used for the development of laser or light-emitting diode [60]. It would be tremendously useful if smooth planar ZnO NRs films could be used to fabricate optoelectronic devices by conventional photolithography. For this purpose, the PL properties were investigated for these discrete NRs and nanorod films. Figure 11 is the comparison of the PL results of ZnO discrete NRs and nanorod film measured at room temperature. For the ZnO nanorod films, one strong and sharp peak centered at

378 nm and several weak blue emission peaks at 422, 450 and 484 nm were found. The emission at 378 nm (3.3 eV) corresponds to the electron transition from the localized level slightly below the conduction band to the valence band of ZnO [61]. A large well-defined band-to-band emission and small defect-related band (420-500nm) at room temperature indicates that the ZnO materials have good crystallinity and relatively high purity [62]. The larger peak for the dense film compared to that of the discrete NRs implies that nanorod films have better interface properties. Furthermore, the side surfaces of NRs exposed to air disappears once they form a dense film, resulting in a large band-to-band emission.

The PL properties of the samples annealed in the temperatures between 200 and 500 °C for 1 hr in air were also investigated with the results shown in figures 11(b) and 11(c) for the discrete NRs and continuous film, respectively. The peak intensities for the band emission were increased significantly after annealing at 200 °C and 300 °C, whereas those annealed at temperatures ≥ 400 °C showed a significant deterioration. The improvement in the PL intensity is more significant for the discrete NRs as the annealing removes the absorbed oxygen at the side surfaces of the NRs and minimizes the non-radiation recombination through surface states etc, leading to an increased PL intensity [63]. However, the PL intensity for the nanorod films only changed slightly after annealing as shown in figure 11(c), indicating the as-grown nanorod films already have much better optical property, less absorbed oxygen at the boundaries of NRs or less interface state effect. A higher PL intensity of the discrete NRs than the films can be mainly attributed to the PL emission from the side of NRs which is not useful for optoelectronic devices. This has been eliminated in the nanorod films. The room-temperature PL results show that the nanorod films have the merit of NRs for optoelectronic devices.

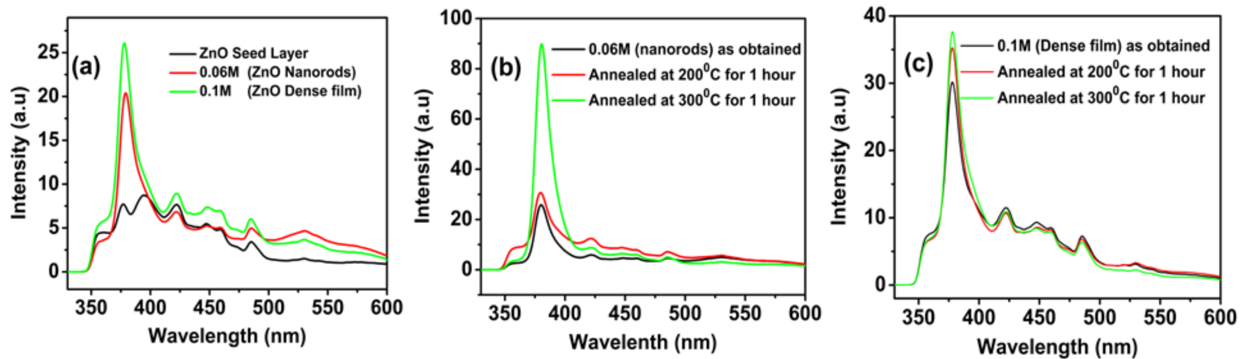

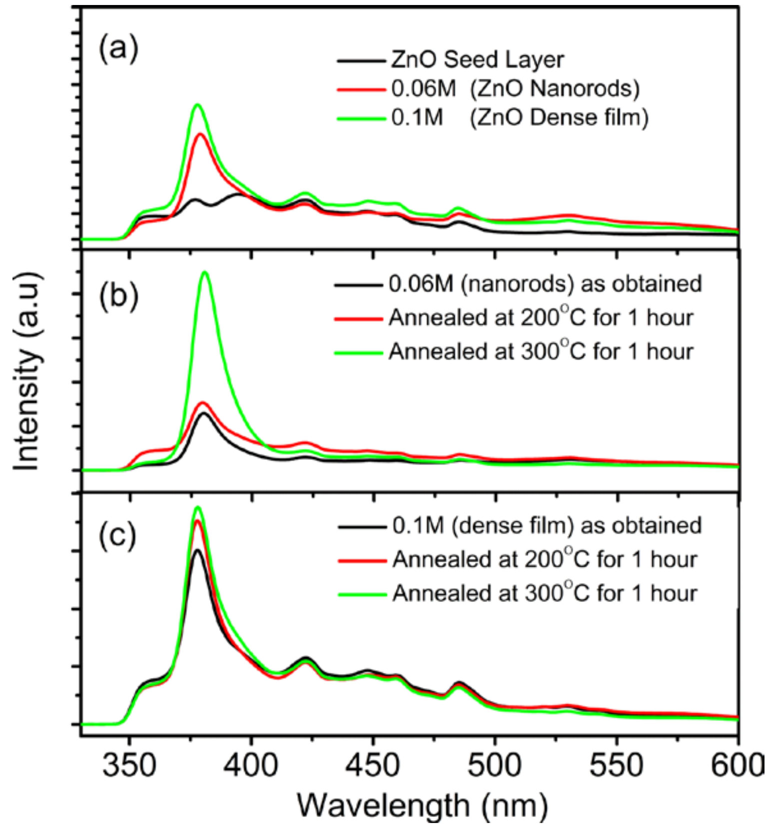

Figure 11. (a) Photoluminescence of ZnO NRs and dense film, showing strong emission from the band gap of the material, (b) PL of ZnO NRs [figure 2(c)] after annealing and (c) PL of ZnO thinfilms [figure 2(e)] after annealing.

3.6 SAW device application

In order to demonstrate the suitability of the smooth nanorod films for large area device applications by planar process fabrication, the nanorod films have been used to fabricate SAW devices. Figure 12 shows SEM images of the fabricated SAW devices and the detailed IDT electrodes. The device surface is very smooth, free of voids and particles. The cross sectional SEM images clearly show that vertical columnar structure densely packed ZnO nanorod structures along (0002) direction. The thickness of the film of the SEM images looks less than 4 μm due to the angle of the sample holder used for the measurement.

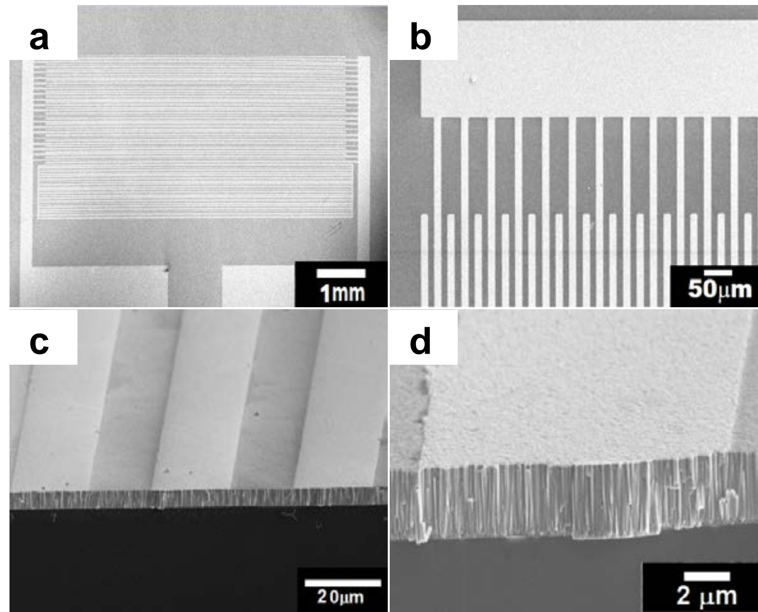

Figure 12. SEM images of the fabricated SAW device, (a) one IDT transducer, (b) detail of the IDT and reflector electrode and (c) and (d) cross sectional view of ZnO nanorod film and the Al electrode.

Figure 13 shows a typical reflection characteristic of a SAW device made on the ZnO nanorod film, showing two resonant peaks at ~120 MHz and 240 MHz, respectively. Assuming these are the fundamental and high mode waves, these resonances correspond to acoustic velocities of 7,744 m/s and 7,680 m/s, respectively. Since ZnO/Si is a bilayer structure, and the acoustic velocity of the SAW devices depends on the thickness of the ZnO piezoelectric film [22]. As ZnO has a lower acoustic velocity (2724 m/s) than that of the Si-substrate, it normally generates a Rayleigh wave of low velocity and a Sezawa wave with higher velocity [64]. The obtained wave velocities of ~7700 m/s for these two peaks, are much higher than that of the Rayleigh wave (~4200 m/s) [22] for the normalized thickness of $hk = 0.39$ (h the thickness of ZnO, $k = 2\pi/\lambda$: wave vector), but compatible to that of the Sezawa wave of ~6800 m/s, therefore the two peaks are believed to be the Sezawa wave and its harmonic mode. It is quite normal that the Rayleigh wave becomes very small when a thick piezoelectric layer is used [22]. In short, we have demonstrated that the ZnO nanorod films can be used to fabricate large area planar SAW devices using the planar process.

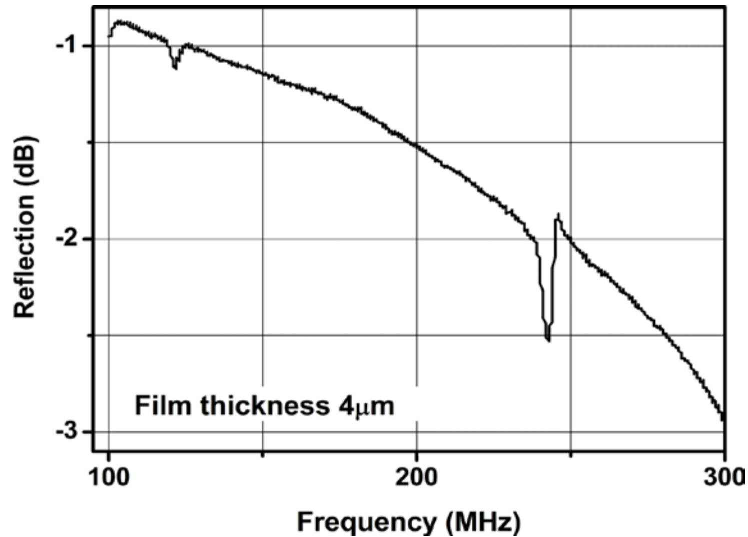

Figure 13. Reflection spectrum of SAW devices made on a solution synthesized ZnO nanorod film with a thickness of 4 μm, showing two resonant peaks of the fundamental and harmonic Sezawa mode resonances.

However, it is found that most ZnO nanorod films synthesized have high electrical conductivity. The resistivity of some nanorod films is in the range of 10^2~10^3 Ω·cm measured between the IDT fingers of the planar SAW devices, which is not well-suitable for piezoelectric applications (minimum requirement for the resistivity is >10^5 Ω·cm). The high conductivity is believed to be responsible for the small amplitude of the reflection signal of the SAW devices shown in figure 13. The high conductivity may be caused by the relatively high concentration of impurities in the solution and high conductivity along the boundaries of NRs even though XPS and PL measurements showed no high concentration impurities in the films. This may be improved by using high purity chemicals for synthesis or further optimization of synthesis process.

4. Conclusions

We have demonstrated unique ZnO nanorod films which consist of densely packed, (0002) oriented ZnO NRs grown by chemical solution method. The chemical concentration, growth temperature and the seed layer have significant effects on the morphology and the density of the NRs. The nanorod films have smooth and continuous surface with roughness less than 5 nm for film thickness up to 4 μm, suitable for device fabrication by planar process. The as-grown nanorod films have stronger band-to-band PL emission than the discrete ZnO NRs owing to reduced surface states, defects and absorbed oxygen on the surface, thus have the potential for optoelectronic devices. We have also fabricated SAW devices using the nanorod films by conventional photolithography process, which show the fundamental and harmonic

Sezawa mode resonances. The results demonstrated the smooth nanorod films have great potential for device applications that will have high performance benefiting from the nanostructured materials, yet can be fabricated by conventional low cost planar process.

Acknowledgements: The authors would like to acknowledge support from the Leverhulme Trust under grant (F/01431/C), the Engineering and Physical Sciences Research Council (EPSRC) under the grant numbers (EP/F06294X/1and EP/F063865/1), and the Knowledge Centre for Materials Chemistry (KCMC), Scottish Sensing Systems Centre (S3C). L. Garcia-Gancedo acknowledges support from the National Natural Science Foundation of China (NSFC) through grant number 61150110485. X-ray photoelectron spectra were obtained at the National EPSRC XPS User's Service (NEXUS) at Newcastle University, an EPSRC Mid-Range Facility.

References

[1] Hiroyuki akaki S 1980 Jpn. J. Appl. Phys. **19** L735.

[2] Wang W, Summers C J and Wang Z L 2004Nano Letters. **4** 423.

[3] Wang Z L and Song J H 2006 Science. **312** 242.

[4] Ruoff R S 1994 Nature. **372** 732.

[5] Ajayan P M, Stephan O, Redlich P and Colliex C 1995 Nature. **375** 564.

[6] Chen Y K, Green M L H and Tsang S C 1996 Chem. Commun. **21** 2489.

[7] Martin C R, 1994 Science. **266**, 1961.

[8] Huber C, Sadoqi M, Huber T and Chacko D 1995 Adv. Mater. **7** 316.

[9] Routkevitch D, Bigioni T, Moskovits M and Xu J M 1996 J. Phys. Chem. B **100** 14037.

[10] Li M, Zhang H Y, Guo C X, Xu J B and Fu X J 2009 Chin. Phys. B **18** 1594–1597.

[11] Govender K, Boyle D S, Brien P O, Binks D, West D and Coleman D 2002 Adv. Mater. **14** 1221.

[12] Park W I and Yi G C 2004 Adv. Mater. **16** 87.

[13] Yeh P H, Li Z and Wang Z L 2009 Adv. Mater. **21** 4975.

[14] Konenkamp R, Word R C and Schlegel C 2004 Appl. Phys. Lett. **85** 6004.

[15] Liu J, Fei P, Zhou J, Tummala R and Wang Z L 2008 Appl. Phys. Lett. **92** 173105.

[16] Iijima S, 1991 Nature. **354** 56.

[17] D. Singh, A.A.Narasimulu, L. Garcia-Gancedo, Y.Q. Fu, T. Hasan, S.S. Lin, J. Geng, G. Shao and J.K. Luo, J. Mater. Chem. DOI: 10.1039/c3tc00873h

[18]Janotti A and Van de Walle C G 2008 Rep. Prog. Phys. **72** 126501.

[19] Willander *et al* 2009 Nanotechnology. **20** 332001.

[20] Wang Z L 2004 Materials Today. **7** 26.

[21] Ozgur U, Alivov Y I, Liu C, Teke A, Reshchikov M A, Dogan S, Avrutin V, Cho S J and Morko H 2005 J. Appl. Phys. **98** 1.

[22] Du X Y, Fu Y Q, Tan S C, Luo J K, Flewitt A J, MilneW I, Lee D S, Park N M, Park J, Choi Y J, Kim S H and Maeng S, 2008 Appl. Phys. Lett. **93** 094105.

[23] Mai L, Kim D H, Yim M and Yoon G 2004 Microwave & Optic. Technol. Lett. **42** 505.

[24] Su Q X, Kirbf P B, Komuro E and Whatmore R K 2000 Proc. IEEE/EIA Int. Freq. Contr. Symp. **2000** 434**.**

[25] Gabl R, Feucht H D, Zeininger H, Eckstein G, Schreiter M, Primig R, Pitzer D and Wersing W 2004 Biosens. & Bioelectron. **19** 615.

[26] Gabl R, Green E, Schreiter M, Feucht H D, Zeininger H, Primig R, Piker D, Eckstein G, Wersing W, Reichl W and Runck J 2003 Proc. IEEE Sensors. **2** 1184.

[27] Pedros J, Garcia-Gancedo L, Ford C J B, Barnes C H W, Griffiths J P, Jones G A C and Flewitt A J 2011 J. Appl. Phys. **110** 103501.

[28] Garcia-Gancedo L, Pedros J, Zhao X B, Ashley G M, Flewitt A J, Milne W I, Ford C J B, Lu J R and Luo J K 2012 Biosens. & Bioelectron. **38** 369.

[29] Fu Y Q, Luo J K, Du X Y, Flewitt A J, Li Y, Markx G H and Walton A J 2010 Sens. & Actuat. B. **143** 606.

[30] Fu Y Q, Garcia-Gancedo L, Pang H F, Porro S, Gu Y W, Luo J K, Zu X T, Placido F, Wilson J I B, Flewitt A J and Milne W I 2012 Biomicrofluid. **6** 024105.

[31] Fortunato E, Barquinha P, Pimentel A, Gonçalves A, Marques A, Pereira L and Martins R 2004 Appl. Phys. Lett. **85** 2451.

[32] Liu N S, Fang G J, Zeng W, Long H, Yuan L Y and Zhao X Z 2011 J. Phys. Chem. C. **115** 570.

[33] Wei A, Sun X W, Wang J X, Lei Y, Cai X P, Li C M, Dong Z L and Huang W 2006 Appl. Phys. Lett. **89** 123902.

[34] Zhu G, Yang R, Wang S H and Wang Z L 2010 Nanolett. **10** 3151.

[35] Yuan H and Zhang Y 2004 J. Cryst. Growth. **263** 119.

[36] Heo Y W, Varadarajan V, Kaufman M, Kim K, Norton D P, Ren F and Fleming P H 2002 Appl. Phys. Lett. **81** 3046.

[37] Sun Y, Fuge G M and Ashfold M N R 2004 Chem. Phys. Lett. **396** 21.

[38] Garcia-Gancedo L, Pedros J, Zhu Z, Flewitt A J, Milne W I, Luo J K, and Ford C J B 2012 J. Appl. Phys. **112** 014907.

[39] Chiou W T, Wu W Y and Ting J M 2003 Diam. Relat. Mater. **12** 1841.

[40] Pung S-Y, Choy K L, Hou X, Shan C 2008 Nanotechnology. **19** 435609.

[41] Vayssieres L, Keis K, Lindquist S E and Hagfeldt A 2001 J. Phys. Chem. B. **105** 3350.

[42] O Brien P and Saeed T 1996 J. Knowles, Mater. Chem. **6** 1135.

[43] Andeen D, Kim J H, Lange F F, Goh G and Tripathy S 2006 Adv. Funct. Mater. **16** 799.

[44] Xu S, Lao C, Weintrub B and Wang Z L 2008 J. Mater. Res. **23** 2072.

[45] Qiu J, Li X, Yu W, Gao X, He W, Park S J, Hwang Y H and Kim H K 2008 Thin Solid Films. **517** 626.

[46] Sounart T L, Liu J, Voigt J A, Hsu J W P, Spoerke E D, Tian and Jiang Y 2006 Adv. Funct. Mater. **16** 335.

[47] Andeen D, Loeffler L, Padture N and Lange F 2003 J. Cryst. Growth. **259** 103.

[48] Kokotov M and Hodes G 2009 J. Mater. Chem. **19** 3847.

[49] Izaki M and Omi T 1997 J. Electrochem. Soc. **144** L3.

[50] Puurunen R 2005 J. Appl. Phys. **97** 12301.

[51] Vayssieres L 2003 Adv. Mater. **15** 464.

[52] Govender K, Boyle D S, Kenway P B and Brien P O 2004 J. Mater. Chem. **14** 2575.

[53] Ren Z F, Huang Z P, Xu J W, Wang J H, Bush P, Siegal M P and Provencio P N 1998 Sci. **282**, 1105.

[54] Lee C J, Kim D W, Lee T J, Choi Y C, Park Y S, Lee Y H, Choi W B, Lee N S, Park G S and Kim J M 1999 Chem. Phys. Lett. **312** 461.

[55] Tao Y, Fu M, Zhao A, He D and Wang Y 2010 J. Alloy & Compound. **489** 99.

[56] Luo J K, Fu Y Q, Du X Y, Lee D S, Maeng S, Flewitt A J and Milne W I 2010 Mater. Res. Soc. Symp. Proc. 1222.

[57] Solis-Pomar F, Martinez E, Melendrez M F and Perez-Tijerina E 2011 Nanoscale Res. Lett. **6**, 524.

[58] Garcia-Gancedo L, Pedros J, Flewitt A J, Milne W I, Ashley G M, Luo J K and Ford C J B 2010 Ultrasonics Symposium. 1064.

[59] Futsuhara M, Yoshioka K and Takai O 1998 Thin Solid Films **322**,274.

[60] Jagadish C and Pearton S J, Zinc Oxide Bulk, Thin Films and Nanostructures: Processing, Properties, and Applications, Elsevier. 2006, 600.

[61] Peterson R B, Fields C L and Gregg B A 2004 Langmuir. **20** 5114.

[62] Guo M, Diao P and Cai S 2005 J. Solid State Chem. **178** 1864.

[63] Gfroerer T H 2000 Encyclopedia of Analytical Chemistry. 9209.

[64] Panella V, Carlotti G, Socino G, GioVannini L, Eddrief M, Amimer K and Sebenne C 1997 J. Phys. Condens. Matter. **9** 5575.